Journal of the Korean Nuclear Society
Volume 32, Number 3, pp.235~243, June 2000

Current Conservation Factors for Consistent One-Dimensional Neutronics Modeling

Kibog Lee, Han Gyu Joo, Byung-Oh Cho, and Sung Quun Zee

Korea Atomic Energy Research Institute
150 Dukjin-dong, Yusong-gu, Taejon 305-353, Korea
kblee@kaeri.re.kr

(Received October 29, 1999)

Abstract

A one-dimensional neutronics formulation is established within the framework of the nonlinear analytic nodal method such that it can result in consistent one-dimensional models that produce the same axial information as their corresponding reference three-dimensional models. Consistency is achieved by conserving axial interface currents as well as the planar reaction rates of the three-dimensional case. For current conservation, flux discontinuity is introduced in the solution of the two-node problem. The degree of discontinuity, named the current conservation factor, is determined such that the surface averaged axial current of the reference three-dimensional case can be retrieved from the two-node calculation involving the radially collapsed group constants and the discontinuity factor. The current conservation factors are derived from the analytic nodal method and various core configurations are analyzed to show that the errors in K-eff and power distributions can be reduced by a order of magnitude by the use of the current conservation factor with no significant computational overhead.

Key Words : current conservation factor, 1D kinectics model, 1D-3D consistency, core simulation, radially collapsed group constants, two-node problem, non-linear CMFD

1. Introduction

A three-dimensional (3D) neutronics code can be considered as the ultimate means of achieving high fidelity in the neutronics simulation of the reactor core. Nonetheless, the one-dimensional (1D) neutronics model are often needed to replace the 3D model in many practical circumstances. The needs are two folds; 1) the significant reduction in computing time and 2) circumventing the lack of detailed neutronic data for the 3D model. When the core characteristic parameters are predominant in the axial direction and the radial flux shape has negligible effects on the global behavior such as the cases of uncontrolled bank withdrawal, xenon transient, BWR flow instability etc, 1D models can be useful. In the aspect of high fidelity real time simulation, such

1D models have a great advantage over the 3D models that are required for a spatial kinetics code coupled with the system thermal-hydraulics.

In the case that a 3D model is available and a 1D model is desired for execution time, it should be possible to generate the 1D model through a consistent radial collapsing procedure. The 1D model obtained as such can then exactly reproduce the 3D results at least at the reference conditions on which the 1D model is based. However, this is possible only when the steady state and transient solution methods of the 1D kinetics module are consistent with the base 3D kinetics module. Most radial collapsing methods to generate the 1D cross sections conserve only the axial node average reaction rates. In most 1D kinetics codes [1,2], there are no provisions made for conserving axial currents that will ensure reproducing the reference 3D results in the 1D calculation.

In this paper a new correction factor in a 1D model is proposed that makes the 1D model consistent with the corresponding 3D model. The 1D model is formulated within the framework of the nonlinear analytic nodal method [3]. It will be derived such that surface properties as well as the node average ones are conserved. In the following sections the correction factor called current conservation factor (CCF) is derived for the 1D model consistent with 3D model. The CCF is generated at the same time when the planar 1D cross-sections are collapsed through the base 3D code and tested for three kinds of steady state cases.

2. Derivation of the One-Dimensional Kinetics Solution Method

The 1D kinetics equation can be derived by integrating the 3D time-dependent neutron diffusion equation over the radial domain. The solution of the 1D kinetics equation is relatively simple because it involves only a block tridiagonal linear system which can be solved directly by the Gaussian elimination scheme. In order to retain good spatial solution accuracy and consistency, the nonlinear analytic nodal method (ANM) implemented in the base 3D code PARCS[3] is used in the 1D solver. The 1D kinetics equation is rigorously derived and the planar averaged group constants are defined. During the derivation, CCF is introduced which guarantees the same axial neutron currents to be obtained from the 1D equation as the 3D reference values. With the planar averaged group constants and CCF's, it becomes possible to reproduce the 3D reference solution from the 1D model. In order to obtain the planar cross-sections as functions of state parameters such as fuel temperature, moderator density and boron concentration, a generalized tabular cross-section representation scheme is considered. It is possible to simulate the reactor core with these 1D cross sections. The detailed solution methods for the eigenvalue and the transient fixed source problems as well as the temporal discretization methods are omitted here since they are already documented well in the reference [3].

2.1. Derivation of the One-Dimensional Kinetics Equation

The 3D time-dependent two-group neutron diffusion equation in Cartesian coordinate reads:

$$\frac{1}{v_g}\frac{\partial \phi_g}{\partial t} = Q_g - \left(\frac{\partial J_{gx}}{\partial x} + \frac{\partial J_{gy}}{\partial y} + \frac{\partial J_{gz}}{\partial z} + \Sigma_{rg}\phi_g \right) \quad (1)$$

where

$$J_{gu} = -D_g \frac{\partial \phi_g}{\partial u} \quad (2)$$

and

$$Q_g = \begin{cases} (1-\beta)(\nu\Sigma_{f1}\phi_1 + \nu\Sigma_{f2}\phi_2) + \sum_{k=1}^{K} \lambda_k C_k, & g = 1 \\ \Sigma_{12}\phi_1, & g = 2. \end{cases} \quad (3)$$

Before integrating Eq. (1) over the radial domain, we factorize the flux into two independent functions, which are defined as the 1D flux (φ) and radial shape function (Φ), respectively, as the following:

$$\phi_g(x,y,z,t) = \varphi_g(z,t)\Phi_g(x,y,z,t). \quad (4)$$

The integration of the left hand side (LHS) of Eq. (1) can then be performed using the factorized flux:

$$\begin{aligned}\int_A \frac{1}{v_g}\frac{\partial \phi_g}{\partial t}dA &= \int_A \frac{1}{v_g}\left(\Phi_g\frac{\partial \varphi_g}{\partial t}+\varphi_g\frac{\partial \Phi_g}{\partial t}\right)dA \\ &= \frac{\partial \varphi_g}{\partial t}\int_A \frac{\Phi_g}{v_g}dA+\varphi_g\frac{\partial}{\partial t}\int_A \frac{\Phi_g}{v_g}dA\end{aligned} \quad (5)$$

In the above derivation, it was assumed that the neutron velocities are time-independent. Since Eq. (4) is an arbitrary factorization, it is possible to impose a constraint on the radial shape function to make the factorization unique. The constraint is chosen such that Eq. (5) can be simplified. Namely,

$$\int_A \frac{\Phi_g}{v_g}dA = \frac{A}{\bar{v}_g(z)} \equiv \int_A \frac{1}{v_g(x,y)}dA \quad (6)$$

where A is the area of the radial domain. The second term on the right hand side(RHS) in Eq. (5) vanishes because the integral term is constant over time and the LHS term reduces to:

$$\int_A \frac{1}{v_g}\frac{\partial \phi_g}{\partial t}dA = \frac{A}{\bar{v}_g}\frac{\partial \varphi_g}{\partial t}. \quad (7)$$

The integration of the removal term on the RHS of Eq. (1) becomes:

$$\int_A \Sigma_{rg}\phi_g dA = \varphi_g\int_A \Sigma_{rg}\Phi dA = A\bar{\Sigma}_{rg}\varphi_g. \quad (8)$$

where the planar averaged removal cross-section is defined as:

$$\bar{\Sigma}_{rg} \equiv \frac{1}{A}\int_A \Sigma_{rg}\Phi_g dA. \quad (9)$$

The other types of planar averaged cross-sections appearing in the source terms (Q_g) can be defined similarly.

The integration of the radial leakage term is simplified by the Gauss theorem as:

$$\begin{aligned}\int_A\left(\frac{\partial J_{gx}}{\partial x}+\frac{\partial J_{gy}}{\partial y}\right)dA &= \oint_B J_{gx}dy+\oint_B J_{gy}dx \\ &= \varphi_g\left(\oint_B -D_g\frac{\partial \Phi_g}{\partial x}dy+\oint_B -D_g\frac{\partial \Phi_g}{\partial y}dx\right) = A\Sigma_{Lg}\varphi_g\end{aligned} \quad (10)$$

where is the leakage cross-section defined as:

$$\Sigma_{Lg} = \frac{1}{A\varphi_g}\left(\oint_B J_{gx}dy+\oint_B J_{gy}dx\right). \quad (11)$$

The integration of the axial leakage term proceeds first by decomposing the axial current term as:

$$J_{gz} = -D_g\frac{\partial \phi_g}{\partial z} = -D_g\left(\varphi_g\frac{\partial \Phi_g}{\partial z}+\Phi_g\frac{\partial \varphi_g}{\partial z}\right). \quad (12)$$

The integration now yields:

$$\begin{aligned}\int_A \frac{\partial J_{gz}}{\partial z}dA &= \frac{\partial}{\partial z}\int_A -D_g\left(\Phi_g\frac{\partial \varphi_g}{\partial z}+\varphi_g\frac{\partial \Phi_g}{\partial z}\right)dA \\ &= -\frac{\partial}{\partial z}\int_A D_g\Phi_g dA\frac{\partial \varphi_g}{\partial z}-\frac{\partial}{\partial z}\left(\varphi_g\int_A D_g\frac{\partial \Phi_g}{\partial z}dA\right).\end{aligned} \quad (13)$$

The first term in the RHS of Eq. (13) can be simplified by introducing the planar averaged diffusion coefficient defined as:

$$\bar{D}_g \equiv \frac{1}{A}\int D_g\Phi_g dA. \quad (14)$$

The second term is, however, not easy to simplify. This term would be zero if $\frac{\partial \Phi_g}{\partial z} = 0$, namely, the radial flux shape is uniform over the axial direction, which is not the normal case. By keeping this term explicitly by the following definition of shape dependent current:

$$\tilde{J}_g \equiv -\frac{\varphi_g}{A}\int_A D_g \frac{\partial \Phi_g}{\partial z} dA \,. \tag{15}$$

Eq. (13) reduces to:

$$\int_A \frac{\partial J_{gz}}{\partial z} dA = A\frac{\partial}{\partial z}\left(\bar{J}_g + \tilde{J}_g\right) \tag{16}$$

where

$$\bar{J}_g \equiv -\bar{D}_g \frac{\partial \varphi_g}{\partial z} \,. \tag{17}$$

By using Eqs. (7), (8), (10), and (16), the 1D kinetics equation is now obtained as follows (after removing A from both sides):

$$\frac{1}{\bar{v}_g}\frac{\partial \varphi_g}{\partial t} = \bar{Q}_g - \left(\hat{\Sigma}_{rg}\varphi_g + \frac{\partial}{\partial z}\hat{J}_g\right). \tag{18}$$

where the effective removal cross-section, $\hat{\Sigma}_{rg}$, is defined as follows by adding the radial leakage cross-section:

$$\hat{\Sigma}_{rg} \equiv \bar{\Sigma}_{rg} + \Sigma_{Lg} \tag{19}$$

and the total axial current, $\hat{J}_g$, combines both components of the current, i.e. :

$$\hat{J}_g \equiv \bar{J}_g + \tilde{J}_g \,. \tag{20}$$

When a flux distribution is available from a reference 3D calculation, the planar averaged group constants can be obtained by evaluating Eqs. (6), (9), (11) and (14) for each plane. If the current due to the difference in the radial shape ($\tilde{J}_g$), which is small compared to the current due to the difference in the 1D flux ($\bar{J}_g$), is neglected, then Eq. (18) can be solved for the 1D flux, φ_g. In such case, however, it is not possible to exactly reproduce the 3D base values of the eigenvalue and the axial flux distribution in the 1D calculation.

A problem arises when $\tilde{J}_g$ is explicitly considered. Since this term does not contain the derivative of the 1D flux as identified in Eq. (15), inclusion of this term makes Eq. (18) no longer a diffusion equation. Moreover, since this term involves $\frac{\partial \Phi_g}{\partial z}$, which can not be evaluated in normal 3D nodal calculations, defining a collapsed group constant for the integral in Eq. (15) is not possible. In order to overcome this problem in the framework of the nonlinear nodal method, the concept of flux discontinuity is introduced here such that the total axial current ($\hat{J}_g$) determined in a 3D reference calculation is conserved in the 1D nodal calculation. With the discontinuity factor whose definition is detailed in the next section, it now becomes possible to exactly reproduce the 3D results in the 1D calculation at least at the reference condition and the 1D model can then be applied to other perturbed states.

2.2. Two-Node Problem to Determine Current Conservation Factor

Suppose two neighboring planes for which the planar averaged group constant, fluxes, and interface currents were obtained from a 3D nodal calculation. For these two planes, it is possible to formulate a two-node problem to determine the nodal coupling relation which is used to represent the interface current in terms of two node (or planar) averaged fluxes as:

$$J_g = -\tilde{D}_g\left(\varphi_g^t - \varphi_g^b\right) - \hat{D}_g\left(\varphi_g^t + \varphi_g^b\right) \tag{21}$$

$$\tilde{D}_g = \frac{2\bar{D}_g^t \bar{D}_g^b}{\bar{D}_g^t \Delta h_z^b + \bar{D}_g^b \Delta h_z^t} \tag{22}$$

where the superscripts t and b stand for top and bottom node of the two nodes, respectively, and $\tilde{D}_g$ means the base nodal coupling coefficients based on finite difference approximation. In normal two-node problem, the interface current

as well as the correctional nodal coupling coefficient (CNCC), $\hat{D}_g$, is the free parameter to be determined from the two-node nodal calculation. In order to solve the normal two-node problem, four constraints are imposed per group. They are two node average fluxes and flux and current continuity at the interface. In a two-node problem, however, the interface current is not a free parameter, rather it is considered as an additional constraint.

The two-group ANM solution for a node is given by the following (refer to Section 4.2 of the reference [3] for the details of the derivation of the ANM solution):

$$\begin{aligned}\begin{bmatrix}\varphi_1(u)\\ \varphi_2(u)\end{bmatrix} &= \begin{bmatrix}\varphi_1^H(u)+\varphi_1^P(u)\\ \varphi_2^H(u)+\varphi_2^P(u)\end{bmatrix}\\ &= \begin{bmatrix} r & s\\ 1 & 1\end{bmatrix}\begin{bmatrix} a_{21}sn(\kappa u)+a_{22}cn(\kappa u)\\ a_{23}sn(\mu u)+a_{24}cn(\mu u)\end{bmatrix}\\ &\quad + \begin{bmatrix} c_{10}+c_{11}f_1(\xi)+c_{12}f_2(\xi)\\ c_{20}+c_{21}f_1(\xi)+c_{22}f_2(\xi)\end{bmatrix}, \quad u = x, y, z.\end{aligned} \tag{23}$$

In the above equation, the c coefficients are determined by the transverse leakage and/or the transient fixed source, which are zero in the 1D steady-state case. The basis functions above are represented concisely in terms of the two generic functions defined below and here the first argument, m, signifies the mode of buckling:

$$sn(m,\lambda k_\infty,u) \ \ or \ \ cn(m,\lambda k_\infty,u) \equiv \begin{cases}\sin(u) \ \ or \ \ \cos(u) & ,if\ m=0\ and\ \lambda k_\infty > 1\\ u \ \ or \ \ 1 & ,if\ m=0\ and\ \lambda k_\infty = 1\\ \sinh(u) \ \ or \ \ \cosh(u) & ,if\ m=1 \ \ or \ \ \lambda k_\infty < 1\end{cases} \tag{24}$$

In a two-node problem, there are then eight coefficients (2*4 a's) to be determined. In order to determine them uniquely, the eight constraint conditions must be specified and two of them are the flux continuity condition for the two groups which reads (the others are four node-average flux constraints - 2 nodes x 2 groups - and two current continuity conditions - 2 groups):

$$\zeta_g^b \varphi_g^b\left(\frac{h_z^b}{2}\right) = \zeta_g^t \varphi_g^t\left(-\frac{h_z^t}{2}\right) \tag{25}$$

where ζ_g is the discontinuity factor that is assumed to be known in normal two-node calculations.

If the two interface currents (one for each group) are added as the additional condition in the two-node problem, then two additional unknowns should be introduced. For this purpose, it is possible to represent the discontinuity factors as follows:

$$\zeta_g^b = 1-\varepsilon_g \quad ; \quad \zeta_g^t = 1-\varepsilon_g \tag{26}$$

and to take ε_g, which is called as CCF , as the additional unknown for each group. The ten unknowns can then be simultaneously determined by imposing the ten constraints.

The homogeneous solution for the two node problem (note that in the 1D steady-state problem, there is no particular solution because the transverse leakage is zero) can be represented as follows in terms of the several basis functions which differs depending on the magnitude of k_∞:

$$\varphi_g^H(z) \in \begin{cases}\{\sin(\kappa z),\cos(\kappa z),\sinh(\mu z),\cosh(\mu z)\} & ,\ k_\infty > k_{eff}\\ \{z,1,\sinh(\mu z),\cosh(\mu z)\} & ,\ k_\infty = k_{eff}\\ \{\sinh(\kappa z),\cosh(\kappa z),\sinh(\mu z),\cosh(\mu z)\}, & k_\infty < k_{eff}\end{cases} \tag{27}$$

In a two-node problem, the homogeneous solution can be compactly represented as:

$$\begin{bmatrix}\varphi_1^q(z)\\ \varphi_2^q(z)\end{bmatrix} = \begin{bmatrix} r^q & s^q\\ 1 & 1\end{bmatrix}\begin{bmatrix} a_1^q sn(\kappa^q z)+a_2^q cn(\kappa^q z)\\ a_3^q sn(\mu^q z)+a_4^q cn(\mu^q z)\end{bmatrix} \quad for \ \ q=b \ or \ t \tag{28}$$

The total 10 unknowns composed of 8 coefficients of the two nodes and 2 CCF' s can be solved with the following constraints:

1) node average fluxes conservation:

$$\bar{\varphi}_g^q = \frac{1}{h^q}\int_{-h^q/2}^{h^q/2}\varphi_g^q(z)dz \quad for \ \ q=b,t; \ \ g=1,2. \tag{29}$$

2) surface average current conservation at the interface:

$$\bar{J}_g^{3D}(z) = -\bar{D}_g^b(z)\frac{d}{dz}\varphi_g^b(z)\Big|_{z=h^b/2} = -\bar{D}_g^t(z)\frac{d}{dz}\varphi_g^t(z)\Big|_{z=-h^t/2}. \quad (30)$$

3) flux continuity using CCF factors at the interface:

$$(1-\varepsilon_g)\varphi_g^b\left(\frac{h_z^b}{2}\right) = (1+\varepsilon_g)\varphi_g^t\left(-\frac{h_z^t}{2}\right). \quad (31)$$

Note that there are additional constraints in Eq. (30) which require the current determined in the two node problem to be the same as the average current obtained from the reference 3D calculation. The above constraints constitute 10 equations that can be solved for 10 unknowns.

The final solution form should be different depending on the basis function which is determined by the node properties. Here, the solution is provided only for the case that the base functions are sin(z) and cos(z) corresponding to m=0, λk_∞>1. The eight coefficients determined from the simultaneous solution of the 10 equations are as follows:

$$a_1^b = \frac{\sec(h^b\kappa^b/2)(2\bar{D}_1^b\bar{J}_2^{3D}s^b + \bar{D}_2^b(-2\bar{J}_1^{3D} + \bar{D}_1^b h^b(\kappa^b)^2(\bar{\varphi}_1^b - s^b\bar{\varphi}_2^b)))}{2\bar{D}_1^b\bar{D}_2^b(r^b - s^b)\kappa^b}, \quad (32)$$

$$a_1^t = \frac{\sec(h^t\kappa^t/2)(2\bar{D}_1^t\bar{J}_2^{3D}s^t + \bar{D}_2^t(-2\bar{J}_1^{3D} + \bar{D}_1^t h^t(\kappa^t)^2(-\bar{\varphi}_1^t + s^t\bar{\varphi}_2^t)))}{2\bar{D}_1^t\bar{D}_2^t(r^t - s^t)\kappa^t}, \quad (33)$$

$$a_3^b = \frac{\sec h(h^b\mu^b/2)(-2\bar{D}_1^b\bar{J}_2^{3D}r^b + \bar{D}_2^b(2\bar{J}_1^{3D} + \bar{D}_1^b h^b(\mu^b)^2(\bar{\varphi}_1^b - r^b\bar{\varphi}_2^b))}{2\bar{D}_1^b\bar{D}_2^b(r^b - s^b)\mu^b}, \quad (34)$$

$$a_3^t = \frac{\sec h(h^t\mu^t/2)(-2\bar{D}_1^t\bar{J}_2^{3D}r^t + \bar{D}_2^t(2\bar{J}_1^{3D} + \bar{D}_1^t h^t(\mu^t)^2(-\bar{\varphi}_1^t + r^t\bar{\varphi}_2^t)))}{2\bar{D}_1^t\bar{D}_2^t(r^t - s^t)\mu^t}, \quad (35)$$

$$a_2^b = \frac{\csc(h^b\kappa^b/2)h^b\kappa^b(\bar{\varphi}_1^b - s^b\bar{\varphi}_2^b)))}{2(r^b - s^b)}, \quad (36)$$

$$a_2^t = \frac{\csc(h^t\kappa^t/2)h^t\kappa^t(\bar{\varphi}_1^t - s^t\bar{\varphi}_2^t)))}{2(r^t - s^t)}, \quad (37)$$

$$a_4^b = \frac{\csc h(h^b\mu^b/2)h^b\mu^b(-\bar{\varphi}_1^b + r^b\bar{\varphi}_2^b)))}{2(r^b - s^b)}, \quad (38)$$

$$a_4^t = \frac{\csc h(h^t\mu^t/2)h^t\mu^t(-\bar{\varphi}_1^t + r^t\bar{\varphi}_2^t)))}{2(r^t - s^t)}, \quad (39)$$

ained

$$\varepsilon_g = \frac{\varphi_g^b(h^b/2) - \varphi_g^t(-h^t/2)}{\varphi_g^b(h^b/2) + \varphi_g^t(-h^t/2)}, \quad g = 1,2 \quad (40)$$

3. Test Problems

CCF values derived in the previous section are generated when the 1D cross-section set is prepared with planar collapsed cross-section. And they are used when solving the intra nodal flux distribution in a two node problem kernel of 1D model.

In order to test the effect of CCF, three kinds

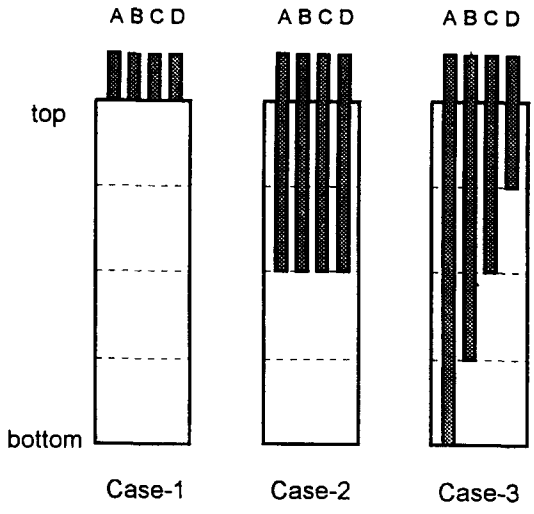

Fig. 1. Three Test Cases

Table 1. Sample of the CCF Values

Node	Case-1		Case-2		Case-3	
No.	CCF-1	CCF-2	CCF-1	CCF-2	CCF-1	CCF-2
2	3.922047E-02	3.792532E-02	3.932028E-02	3.799754E-02	4.095733E-02	3.965351E-02
3	1.402784E-03	1.540256E-03	1.401115E-03	1.526394E-03	1.460416E-03	1.692759E-03
4	6.207732E-04	1.281259E-03	6.067341E-04	1.238928E-03	6.193009E-04	1.354002E-03
5	7.097761E-04	1.247093E-03	6.572262E-04	1.142919E-03	6.553792E-04	1.406484E-03
6	4.847944E-04	7.626906E-04	3.002599E-04	4.897273E-04	5.145261E-05	6.294915E-04
7	2.859150E-04	4.469273E-04	5.295197E-05	9.835972E-05	-4.922900E-04	-3.372619E-05
8	1.689825E-04	2.624045E-04	-1.926969E-04	-2.936846E-04	-5.825792E-04	-8.159370E-04
9	7.776116E-05	1.208078E-04	1.470752E-04	3.410101E-04	-4.909438E-04	-1.378600E-03
10	-2.420514E-06	-3.479503E-06	2.128189E-04	1.172492E-03	-1.158163E-03	-2.673722E-03
11	-8.231506E-05	-1.273399E-04	-3.193745E-03	-7.698134E-03	-2.277768E-03	-3.021050E-03
12	-1.749327E-04	-2.703663E-04	-9.997496E-03	-1.439397E-02	-2.921803E-03	-3.646835E-03
13	-2.939006E-04	-4.556907E-04	-5.189781E-03	-8.247424E-03	-2.120458E-03	-2.667255E-03
14	-4.968247E-04	-7.686452E-04	-7.415104E-03	-1.050758E-02	-1.097869E-03	-1.046316E-03
15	-7.109716E-04	-1.232297E-03	-2.313249E-03	-4.181173E-03	-2.601829E-03	-5.937549E-03
16	-6.252996E-04	-1.352798E-03	-9.782316E-04	-2.300859E-03	-1.345732E-03	-3.896898E-03
17	-1.613005E-03	-1.334228E-03	-2.025886E-03	-3.963753E-03	-2.356987E-03	-5.068253E-03
18	-3.987261E-02	-3.330637E-02	-4.307671E-02	-3.804341E-02	-4.868531E-02	-4.426072E-02

Table 2. Comparison of the Core Eigenvalue(K-eff) at a Steady State

Method		Case-1	Case-2	Case-3
3D reference	K-eff	1.087519	1.078697	1.075649
1D without CCF	K-eff	1.087554	1.078791	1.075771
	Error(pcm)*	-3.5	-9.4	-12.2
1D with CCF	K-eff	1.087522	1.078706	1.075660
	Error(pcm)*	-0.3	-0.9	-1.1

* : Error = (3D - 1D)*100000

Table 3. Comparison of Maximum Axial Power at a Steady State

Method		Case-1	Case-2	Case-3
3D reference	Peak	1.5097(9)	2.5804(7)	2.2552(7)
1D without CCF	Peak	1.5058(9)	2.5727(7)	2.2506(7)
	Error(%) *	-0.256	-0.300	-0.202
1D with CCF	Peak	1.5092(9)	2.5793(7)	2.2543(7)
	Error(%) **	-0.033	-0.046	-0.039

** : Error = (3D - 1D)/3D*100

(#) means the node number

Table 4. Comparison of Peripheral Node Power at a Steady State

Method		Case-1	Case-2	Case-3
3D reference	Node Power	0.1637(2)	0.4954(2)	0.4776(2)
1D without CCF	Node Power	0.1729(2)	0.5235(2)	0.5072(2)
	Error(%) **	5.591	5.657	6.202
1D with CCF	Node Power	0.1654(2)	0.5005(2)	0.4828(2)
	Error(%) **	1.027	1.024	1.082

Table 5. Comparison of CPU Time(seconds)

Method	Case-1	Case-2	Case-3
3D reference	8.22	8.96	8.41
1D without CCF	0.39	0.49	0.66
1D with CCF	0.44	0.45	0.63

Computer : PC 300MHz Machine

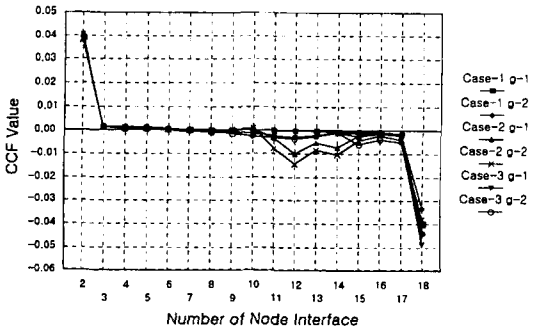

Fig. 2. CCF Values vs. Node Interface for Three Cases

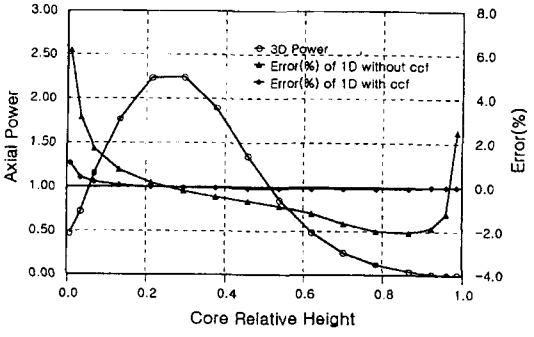

Fig. 3. Comparison of Axial Power Distribution (Case-3)

of steady state calculations are performed. The test core is based on NEACRP benchmark problem[4]. The axial flux(power) distribution is mainly distorted by the control rod insertion, so the test cases are selected as case 1; all rod out case, case 2; rods inserted half to the active core height and case 3; several rods are inserted sequentially. Figure 1 shows the three test cases.

4. Results and Conclusions

Table 1 and Figure 2 show the CCF values obtained from the three test cases. Table 2 shows the results of K-eff values compared with the 3D reference value when the CCF is used and not

used. The errors of K-eff values are reduced about one tenth when using CCF. The axial power distribution from 1D calculation agrees well to that of 3D reference value as shown in Figure 3. Tables 3 and 4 show the comparison results of peak power and peripheral power. The errors of power are decreased to the range of one fifth or tenth in the case using CCF. But as shown in Table 5, the 1D calculation time is very short compared with the 3D calculation time, and there is no additional CPU time due to using CCF in the 1D computation.

With the planar averaged group constants and CCF' s for the specified state, it becomes possible to reproduce the 3D reference solution from the 1D model. Thus the 1D model with CCF can provide more accurate results at the steady state, and the error propagation due to the difference from the initial state will be eliminated. It is expected that the accuracy of the 1D transient calculation can be improved as well with the use of CCF' s provided that the dependence of CCF' s on the control rod configuration is functionalized properly.

5. Acknowledgement

This study has been carried out under the Nuclear R&D Program sponsored by Ministry of Science and Technology of Korea. The authors would like to express their appreciation to Prof. Thomas J. Downar of PURDUE University and USNRC for their support.

6. References

1. W. K. Terry and D. W. Nigg, " One-Dimensional Diffusion Theory Kinetics in RELAP5," *Nucl. Sci. Eng.*, **120**, 110-123 (1995).
2. Kibog Lee et al, "Verification of ONED90 Code," *KAERI/TR-396/93*, KAERI, (1993).
3. H. G. Joo et al, "Stabilization Techniques for the Nonlinear Analytic Nodal Method," *Nucl. Sci. Eng.*, **130**, 47 (1998).
4. H. Finnemann et al, "Results of LWR Core Transient Benchmarks," *Proc. Intl. Conf. Math. Meth. Supercomput. Nucl. Appl.*, Karlsruhe, pp. 243-258, April 1993.